

Au- and Pd-Doped SnS₂ Monolayers for Lung Cancer Biomarkers (C₃H₆O, C₆H₆, and C₅H₈) Detection: A Density Functional Theory Investigation

Hongyi Liu and Xuan Luo*



Cite This: *ACS Omega* 2024, 9, 7658–7667



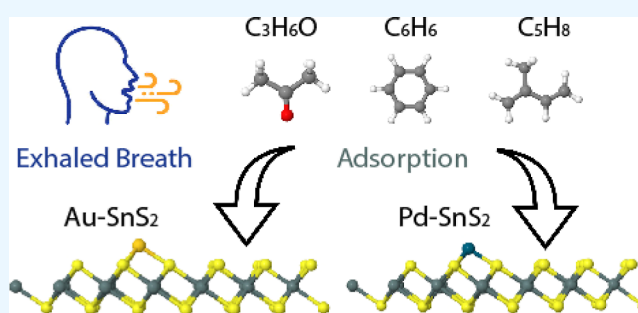
Read Online

ACCESS |

Metrics & More

Article Recommendations

ABSTRACT: An efficient and noninvasive method of sensing lung cancer at an early stage is through detecting its biomarkers in the patient's exhaled breath. Acetone (C₃H₆O), benzene (C₆H₆), and isoprene (C₅H₈) emerged as crucial biomarkers, which were significantly elevated in lung cancer patients. Here, we investigated the adsorption behaviors of the three gas molecules on pristine and transition metal (TM)-doped (Au and Pd) SnS₂ monolayers using the density functional theory (DFT) method. Our findings indicate that both Au- and Pd-doped SnS₂ display higher adsorption energies (−0.53 to −1.313 eV) than that of the pure SnS₂ monolayer (0.031 to 0.066 eV). Specifically, Pd–SnS₂ exhibits smaller adsorption energy compared to that of Au–SnS₂ when capturing C₃H₆O, C₆H₆, and C₅H₈. The estimated recovery times for Pd–SnS₂ (8.016 × 10^{−4} to 16.02 s) are shorter compared to those of Au–SnS₂ (1.11 to 1.14 × 10¹⁰ s), indicating the superior capability of Pd–SnS₂ over Au–SnS₂ as a reversible sensor. Afterward, calculations of band structure, projected density of states (PDOS), and charge transfer were performed, which further substantiates the more promising potentials for Pd-doped SnS₂ monolayer as gas sensors over the others. Overall, our results suggest that Pd–SnS₂ is a better candidate for C₃H₆O, C₆H₆, and C₅H₈ detection over Au–SnS₂ and pristine SnS₂.



1. INTRODUCTION

As the second most prevailing cancer in the world with the highest morbidity and mortality rate among adults, lung cancer poses a great threat to human health, leading to approximately 2.2 million new cases and 1.8 million deaths in the year 2020.^{1–4} Research institutes and pharmaceutical industries have devoted extensive efforts to explore knowledge of lung cancer, including methods of diagnosis and therapeutics. In recent years, technologies such as computed tomographic (CT)⁵ and nuclear magnetic resonance (NMR)⁶ are widely applied in clinical scenarios for early detection of lung cancer. However, those methods are expensive to operate,^{7–9} potentially dangerous to the body of the patients, possible of overdiagnosis,⁵ and can only make a definite diagnosis at an advanced stage of cancer.^{4,10} Due to these drawbacks, a rapid, noninvasive, and cost-effective method to detect lung cancer is valuable. One of the recent developments to constantly monitor the existence of lung cancer is through the detection of lung cancer biomarkers in breath analysis.^{9,11,12} Volatile organic compounds (VOC) such as acetone (C₃H₆O), benzene (C₆H₆), and isoprene (C₅H₈) are typical biomarkers for breath analysis of lung cancer.^{13–16}

One of the major technologies of VOC detection via breath analysis is GC–MS,^{17,18} which is acknowledged as the

benchmark in clinical trials for lung cancer detection in early stages. Nevertheless, it is time consuming and expensive and requires proficient professionals, thus stimulating the need of biosensors for lung cancer biomarkers with rapid and effective detection.^{12,17} Within the past few decades, there is an increasing interest in utilizing nanomaterials for C₃H₆O, C₆H₆, and C₅H₈ sensing due to their naturally active surface, small size and cost-effectiveness.¹⁹ Carbon nanotubes (CNT) have shown high potential for sensing these three gases thanks to their large specific surface area, small tip ratios and high conductivity.^{16,20} Besides, other nanomaterials such as metal–organic frameworks (MOFs) and metal oxide semiconductors (MOS) are also desirable for sensing the three molecules due to their tunability, low cost and small size.^{21–23} Meanwhile, zeolite layers are capable of catalyzing the sensing performance of MOS upon C₃H₆O, C₆H₆, and C₅H₈ gases.²² In recent years, 2D materials have attracted much attention for lung

Received: September 8, 2023
Revised: October 23, 2023
Accepted: November 9, 2023
Published: November 28, 2023



cancer biomarker capturing due to their extremely high surface area–volume ratio, high sensitivity, rapid response, and the smaller size and other characteristics that could not be identified from other nanomaterials.^{17,19}

In 2010, Andre Geim and Konstantin Novoselov were granted the Nobel Prize in Physics for their discovery of the carbon monolayer known as graphene,²⁴ which sparked a new era in the development of gas sensors utilizing 2D monolayers. Since then, the gas sensing properties of graphene-like 2D materials,^{25,26} stanene,²⁷ silicene,^{28,29} transition metal oxides (TMOs),^{30–32} and transition metal dichalcogenides (TMDs)^{10,33–35} have been substantially studied. Thanks to their superior semiconducting behavior, strong reactivity, high carrier mobility, and high surface-to-volume ratio, TMD monolayers, especially MoS₂, MoSe₂, and PtTe₂,^{4,10,15,36,37} have become a focus of attention for gas sensing applications.^{33,38} Similar to TMDs, SnS₂ monolayer possesses desirable semiconducting characteristics with an indirect band gap of 1.57 eV,³⁹ high on/off ratio of 10,^{8,40} and exceptional carrier mobility of 50 m² V⁻¹ s⁻¹^{133,41,42} that are similar to TMD monolayers, indicating its effective application in gas sensing.⁸ Ou's study revealed that the SnS₂ monolayer exhibits favorable sensing abilities for NO₂ gas,⁴³ while another research by Guo also demonstrates SnS₂ monolayer's selectivity and desirable sensitivity toward SF₆ decomposition gases.⁴⁰ Moreover, Zhao et al.⁴⁴ conducted a study that concentrated on the electronic characteristics of S-vacancy defective SnS₂ monolayers, which demonstrates strong interaction with molecules including NO₂, NO, NH₃, H₂O, and CO. Hence, we assert that the SnS₂ monolayer showcases high tunability, and the introduction of transition metal doping offers the potential for significant modifications to the adsorption and gas sensing characteristics of SnS₂ monolayers, thereby facilitating the detection of C₃H₆O, C₆H₆, and C₅H₈ molecules.

Currently, there is limited research on whether pristine and TM-doped SnS₂ are desirable for C₃H₆O, C₆H₆, and C₅H₈ sensing. Previous research investigated Ru-doped SnS₂ as a biosensor for lung cancer biomarker detection.⁸ Nevertheless, its limitation is obvious because of its extremely long recovery time at room temperature and its insufficient attention given to alternative transition metal dopants that have the potential to enhance the sensing capabilities of the SnS₂ layer. Over the past few years, various studies have validated the superb gas-sensing performance of some other TM-doped or TM cluster-doped SnS₂ monolayer.^{42,45–48} Wang and Wang's research validated the enhanced sensing capabilities of Au-doped SnS₂ monolayers for detecting NO₂, NO, CO, CO₂, and NH₃,⁴⁵ while a separate study exhibited favorable adsorption characteristics for C₂H₂ and H₂ molecules on Pd-doped SnS₂ monolayers.⁴⁶ Therefore, our research focuses on the potential of Au- and Pd-doped SnS₂ for sensing the three VOC molecules.

The first-principle calculations based on the density functional theory (DFT)⁴⁹ are utilized in this study to evaluate the effectiveness of pristine, Au-doped, and Pd-doped SnS₂ monolayer to detect C₃H₆O, C₆H₆, and C₅H₈. We conducted computations to analyze the atomic and electronic configurations of pristine Au- and Pd-doped SnS₂ monolayers. Afterward, the calculated results of the VOCs' adsorption on the pristine, Au- and Pd-doped SnS₂ monolayers are compared and analyzed to find a suitable sensor for the three VOCs.

2. METHOD

2.1. Computational Details. The density functional theory (DFT)⁴⁹ incorporated into the ABINIT package⁵⁰ implements the generalized gradient approximation (GGA)⁵¹ exchange–correlation functionals with a Perdew–Burke–Ernzerhof (PBE) format. The projected augmented wave (PAW) method⁵² is used to produce pseudopotentials using the AtomPAW code.⁵³ The electron configurations of hydrogen (H), carbon (C), oxygen (O), tin (Sn), sulfur (S), gold (Au), and palladium (Pd) are 1s¹, [He]2s²2p², [He]-2s²2p⁴, [Kr]4d¹⁰5s²5p², [Ne]3s²3p⁴, [Xe 4f¹⁴]5d¹⁰6s¹, and [Ar 3d¹⁰]4s²4p⁶5s¹4d⁹ respectively. The radius cutoffs of these atoms are 1.0, 1.5, 1.4, 2.5, 1.0, 2.5, and 2.5 bohrs, respectively.

In the total energy calculation, the self-consistent field (SCF) cycle will stop once the total energy difference is less than 1.0 × 10⁻¹⁰ Ha twice consecutively. Besides, the convergence of kinetic energy cutoff, Monkhorst–Pack⁵⁴ *k*-point grids, and vacuum layer is also calculated. The convergence criterion is fulfilled when the difference in total energy is smaller than 0.0001 Ha (0.003 eV) between two consecutive data sets.

Using the Broyden–Fletcher–Goldfarb–Shanno minimization (BFGS),⁵⁵ we performed structural optimization of the three gas molecules, pristine, Au- and Pd-doped monolayers, and the complex systems. The tolerance for the maximum force of each atom is less than 2.0 × 10⁻⁴ Ha/bohr (0.01 eV/Å). The SCF cycle will be terminated once the force difference is smaller than 2.0 × 10⁻⁵ twice consecutively.

2.2. Atomic Structures. We started with structural optimization calculations of the C₃H₆O, C₆H₆, and C₅H₈ molecules. We first optimized SnS₂ as a primitive cell and then established a 4 × 4 × 1 monolayer from this primitive cell, comprising 16 Sn atoms and 32 S atoms with the Sn atoms located between two layers of S atoms. Afterward, Au- and Pd-doped SnS₂ was constructed by placing the Au or Pd dopant interstitially above the hollow site of the 4 × 4 monolayer. Eventually, we placed the C₃H₆O, C₆H₆, and C₅H₈ molecules onto the different SnS₂ monolayers and then optimized the structure. To prevent interactions between adjacent unit cells during the adsorption of three VOCs onto the monolayers, a vacuum layer of 30 bohrs is established.

2.3. Energy Calculation. When the C₃H₆O, C₆H₆, and C₅H₈ are adsorbed on top of the monolayer, the adsorption energy^{56–64} is given as

$$E_{\text{ad}} = E_{\text{mol+monolayer}} - E_{\text{monolayer}} - E_{\text{mol}} \quad (1)$$

in which E_{ad} , $E_{\text{mol+monolayer}}$, $E_{\text{monolayer}}$, and E_{mol} represent the adsorption energy, the total energy of gas–SnS₂ system, SnS₂ monolayer, and the gaseous molecule, respectively.

2.4. Electronic Structure. **2.4.1. Band Structure.** First, we used the relaxed positions of the atoms from the complex structure of C₃H₆O, C₆H₆, and C₅H₈ adsorption on pristine, Au- and Pd-doped SnS₂ monolayer. Next, employing the converged charge density values obtained in the preceding stage, we computed the band structures along the high symmetry *k*-points $\Gamma(0, 0, 0)$, $M(1/2, 0, 0)$, $K(1/3, 2/3, 0)$, and $\Gamma(0, 0, 0)$.

2.4.2. Projected Density of States. To analyze the VOC adsorption on pristine Au- and Pd-doped SnS₂ substrates, we conducted calculations of the projected density of states (PDOS) using the tetrahedron method. The atoms chosen for projection are the atoms closest to the site of gas adsorption.

Therefore, the PDOS of the 2p orbital of O in C₃H₆O, the 2p orbital of C in C₆H₆ and C₅H₈, the 3p orbital of S, the 4d orbital of the Pd dopant, or the 5d orbital of the Au dopant were calculated and plotted for VOC adsorbed Au- and Pd-doped SnS₂ systems.

2.4.3. Charge Transfer. The interaction between the VOC molecules and the SnS₂ monolayer is further studied by the calculation of charge transfer between them. The charge transfer^{19,65,66} can be expressed as

$$\Delta\rho = \rho_{\text{mol/surf}} - \rho_{\text{surf}} - \rho_{\text{mol}} \quad (2)$$

in which $\Delta\rho$ represents the net charge transfer, while $\rho_{\text{mol/surf}}$, ρ_{surf} , and ρ_{mol} represent the charge density of the gas–SnS₂ system, SnS₂ monolayer, and the VOC molecule correspondingly. We utilized the cut3d program to process the charge density of the monolayer, molecule, and the molecule–monolayer combined system. Subsequently, we utilized VESTA to generate the isosurfaces representing the difference in charge density.

2.5. Recovery Time, Conductivity, and Sensing Response. To evaluate the reusability of the sensing material, we calculated the recovery time, which is the minimum time for gas desorption from the monolayer, is calculated. The recovery time (τ)^{17,35,47} can be expressed as

$$\tau = \nu^{-1} e^{-E_{\text{ad}}/k_{\text{B}}T} \quad (3)$$

where ν represents the attempt frequency ($\nu = 10^{12} \text{ s}^{-1}$ for visible light^{12,17,47,57}), k_{B} represents the Boltzmann constant ($k_{\text{B}} = 8.617 \times 10^{-5} \text{ eV K}^{-1}$ ^{17,47,57}), and T represents temperature ($T = 300 \text{ K}$ for room temperature¹⁷).

The electrical conductivity (σ)^{4,12,17,36} of the SnS₂ systems can be calculated by

$$\sigma \propto \exp(-E_{\text{g}}/2k_{\text{B}}T) \quad (4)$$

where E_{g} , k_{B} , and T represent the band gap of SnS₂ systems, the Boltzmann constant, and the thermodynamic temperature correspondingly.

Another crucial aspect that influences a gas sensor's effectiveness is the monolayer's sensing response (S)^{4,15}. Sensing response is defined as the variation in electrical resistance prior to and after the adsorption of gases, and it is defined as follows

$$S = \frac{\sigma_{\text{monolayer+mol}}^{-1} - \sigma_{\text{monolayer}}^{-1}}{\sigma_{\text{monolayer}}^{-1}} \quad (5)$$

where $\sigma_{\text{monolayer}}$ and $\sigma_{\text{monolayer+mol}}$ indicate the conductivity of the monolayer and the gas–monolayer system correspondingly.

3. RESULTS AND DISCUSSION

We first analyzed the structural and adsorption properties before and after the adsorption of C₃H₆O, C₆H₆, and C₅H₈ onto the pristine SnS₂ monolayer. To improve the sensing responses toward the three VOC molecules, TM dopants (Au and Pd) are interstitially doped at the hollow site onto the pure substrate. Then, we compared the adsorption energy, recovery time, band structure, sensing responses, PDOS, and charge transfer of Au–SnS₂ and Pd–SnS₂ monolayers to assess their abilities in sensing the three VOC molecules.

3.1. VOCs on Pristine SnS₂. The structural optimization is calculated for the C₃H₆O, C₆H₆, and C₅H₈ molecules, as identified in Figure 1. Table 1 displays the optimized structural

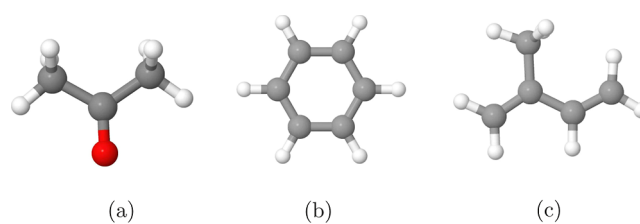


Figure 1. Optimized atomic structure of (a) acetone, (b) benzene, and (c) isoprene. Gray, white, and red colors are used to symbolize C, H, and O atoms, correspondingly.

parameters of the pure SnS₂ monolayer and the three VOC molecules. In the C₃H₆O molecule, the calculated lengths for the C–O and C–C bonds are 1.22 and 1.51 Å correspondingly, while the bond angle of O–C–C measures 121.8°. When examining the C₆H₆ molecule, calculations reveal a C–C bond length of 1.4 Å and a C–C–C angle of 120°. Regarding the C₅H₈ molecule, the optimized lengths are 1.5 and 1.35 Å for C–C_{methyl} and C=C bonds, respectively, accompanied by the bond angle of 119.7° for C=C–C. Figure 2a demonstrates the optimized configurations of the perfect 4 × 4 pristine SnS₂ monolayer. The lattice constant of pristine SnS₂ is 3.7 Å, while the bond length of Sn–S is 2.6 Å (Table 2). The small percentage error listed in Table 1 suggests that our calculated results for the three VOC molecules and pristine SnS₂ monolayer align with prior theoretical and experimental outcomes.^{4,8,39,42,45,67–71}

Figure 3 demonstrates the top and side views of the optimized configurations of the three systems. According to Table 3, the adsorption distances of C₃H₆O, C₆H₆, and C₅H₈ systems are 3.33, 3.83, and 2.97 Å, respectively. Simultaneously, the adsorption energies of C₃H₆O, C₆H₆, and C₅H₈ are 0.066, 0.034, and 0.031 eV respectively. The miniscule positive adsorption energy values signify a nonspontaneous reaction, highlighting that the VOCs will not be adsorbed onto the pristine SnS₂ monolayer. Therefore, pure SnS₂ is not a suitable sensor for C₃H₆O, C₆H₆, and C₅H₈.

3.2. VOCs on Au–SnS₂. For the 4 × 4 × 1 Au–SnS₂ monolayer, the interstitial doping of the Au atom at the hollow site is the most stable site with an adsorption energy of –2.78 eV and can effectively enhance the sensing performance of the pristine SnS₂ monolayer.⁷² The structural optimization of the Au–SnS₂ monolayer is illustrated in Figure 2b, including its top and side view. The lengths of the three Au–S bonds obtained are 2.51, 2.52, and 2.52 Å, respectively. These measurements are consistent with the findings of Gui's study,⁴⁷ which reported an Au–S bond length of 2.547 Å. Meanwhile, the lattice constant of the monolayer is slightly stretched to 3.716 Å, as is evident in Table 2.

Figure 4 illustrates the optimized configurations of the adsorption of three VOCs on the Au–SnS₂ monolayer. The adsorption energies for C₃H₆O, C₆H₆, and C₅H₈ were calculated to be –0.77, –0.717, and –1.313 eV, respectively, as illustrated in Table 4. Simultaneously, the average binding distances for the C₃H₆O, C₆H₆, and C₅H₈ systems were measured to be 2.13, 2.32, and 2.16 Å. Of the three VOC molecules, C₅H₈ exhibits the strongest adsorption onto the layer due to its highest adsorption energy. The significantly reduced binding distances and greater adsorption energies infer much stronger adsorption of the VOCs on Au-doped SnS₂ than on pristine SnS₂. Using eq 3, the recovery times of the C₃H₆O, C₆H₆, and C₅H₈ were estimated to be 8.63, 1.11, and

Table 1. Calculated, Theoretical and Experimental Results for the Structural Parameters of the Three VOC Molecules and the Pure SnS₂ Monolayer [Lattice Constant (*a*) and Sn–S Bond (*d*)] and the Percentage Error between Our Research and the Experiment

	parameters	calculated	other theory	experimental	percentage error (%)
C ₃ H ₆ O	C–O (Å)	1.22	1.22 ⁴	1.14 ⁶⁷	7.02
	C–C (Å)	1.51	1.52 ⁴	1.56 ⁶⁷	3.21
	∠C–C–O (deg)	121.8	N/A	123 ⁶⁷	0.98
C ₆ H ₆	C–C (Å)	1.40	1.40 ⁸	1.399 ⁶⁸	0.07
	∠C–C–C (deg)	120	111.9 ⁶⁸	120 ⁶⁸	0
C ₅ H ₈	C=C (Å)	1.35	1.35 ⁴	1.34 ⁶⁹	0.75
	C–C _{methyl} (Å)	1.5	1.51 ⁴	1.512 ⁶⁹	0.79
	∠C=C–C (deg)	119.7	N/A	N/A	N/A
SnS ₂ monolayer	<i>a</i> (Å)	3.7	3.7 ³⁹	3.647 ⁷⁰	1.45
	<i>d</i> (Å)	2.6	2.59 ⁴⁵	2.572 ⁷¹	1.09

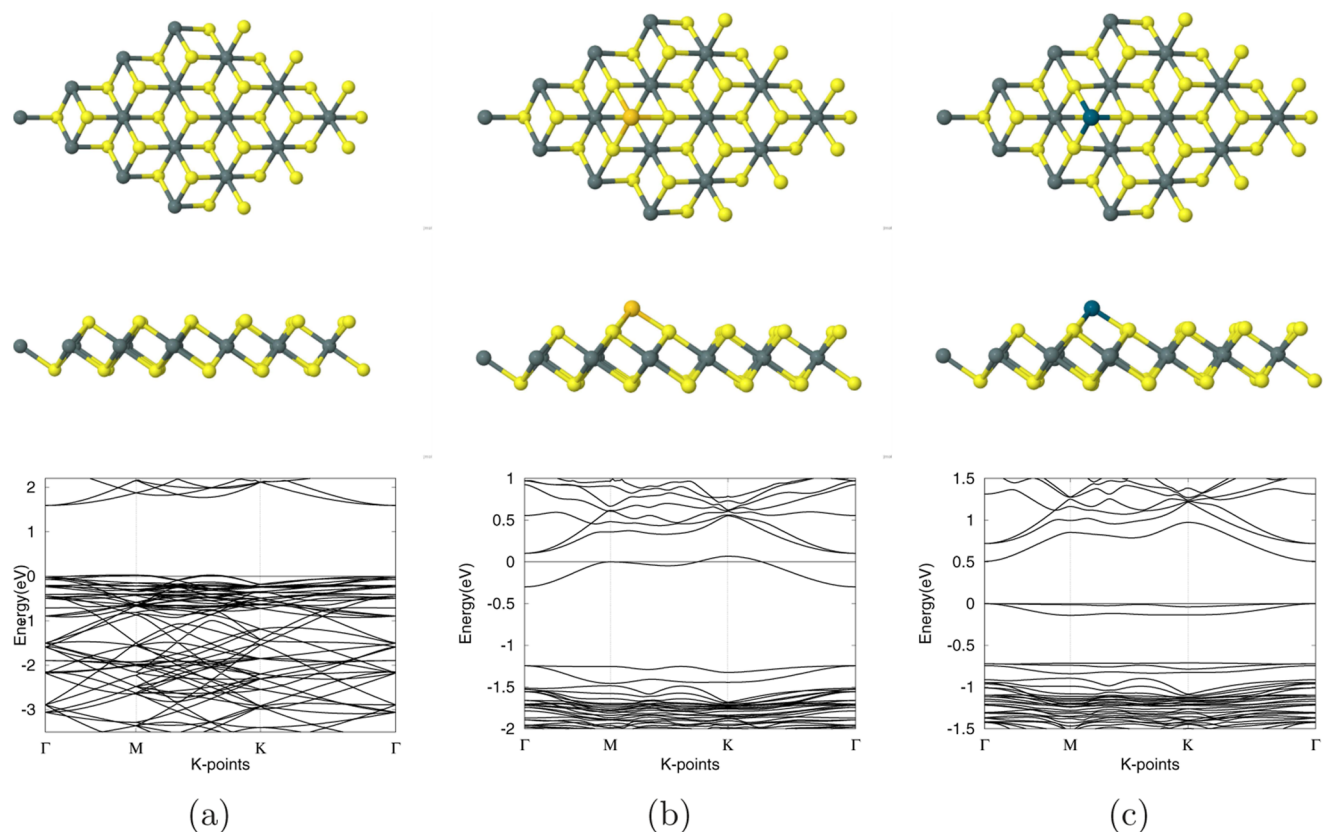


Figure 2. Top and side view and the band structures of (a) pure SnS₂, (b) Au–SnS₂, and (c) Pd–SnS₂ substrates. Top row, middle row, and bottom row represent the top view, side view, and band structure correspondingly. C, H, O, Au, and Pd atoms are represented by gray, white, red, light orange, and indigo colors, respectively.

Table 2. Optimized Structural Parameters for 4 × 4 × 1 SnS₂ Monolayer: Lattice Constant (*a*), Bond Length (*d*) of S–TM, and Band Gap (*E_g*)

configuration	<i>a</i> (Å)	<i>d</i> (Å)	<i>E_g</i> (eV)
pristine SnS ₂	3.7	N/A	1.59
Au–SnS ₂	3.716	2.51	0.035
Pd–SnS ₂	3.72	2.38	0.57

1.143 × 10¹⁰ seconds, respectively. Thus, Au–SnS₂ showcases promising potential as a reversible sensor for C₃H₆O and C₆H₆ due to their short recovery times, while proving itself unsuitable as a sensor for C₅H₈ due to its prolonged desorption time.

After structural optimization, the band structures of Au–SnS₂ before and after the adsorption of three VOC molecules were calculated, as demonstrated in the bottom row of Figure 2 and the upper row of Figure 5. Table 2 shows that following Au-doping, the band gap of the monolayer shrank dramatically to 0.035 eV from 1.59 eV. Upon the adsorption of the three VOC molecules, all systems become metallic as the band gaps are decreased to zero. According to eq 4, the band gap is essential for determining the electrical conductivity of the SnS₂ monolayer. Such small changes in band gap correlate with a small change in conductivity, which indicates Au–SnS₂'s low sensing responses of 49.18% toward the three VOC molecules, as inferred from eq 5.

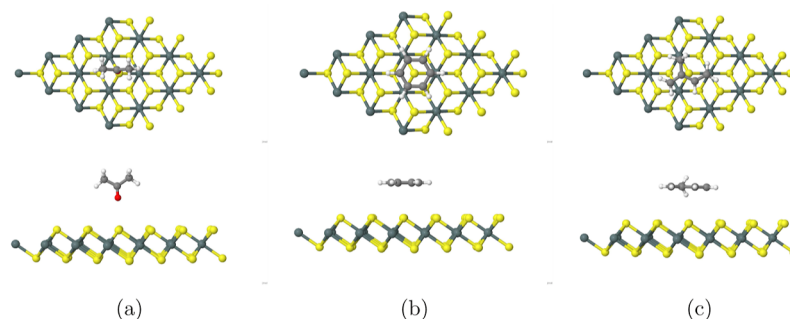


Figure 3. Top and side views of the most stable configurations of (a) C_3H_6O , (b) C_6H_6 , and (c) C_5H_8 adsorption on pure SnS_2 monolayer. The top and bottom rows represent the top and side views of all systems correspondingly. C, H, O, Sn, and S are represented by light gray, white, red, dark gray, and yellow colors, respectively.

Table 3. Adsorption Energy (E_a) and Binding Distance (h) between the VOC Gas and the Monolayer for All VOCs Absorbed on Pristine 4×4 SnS_2 Monolayer

system	E_a (eV)	h (Å)
C_3H_6O on pristine SnS_2	0.066	3.33
C_6H_6 on pristine SnS_2	0.034	3.83
C_5H_8 on pristine SnS_2	0.031	2.97

The PDOS after the adsorption of three VOCs on the Au- SnS_2 monolayer was calculated and graphed, as noted in the bottom row of Figure 5. For the C_3H_6O system, strong hybridization between Au s, Au d, O p, and S p orbitals occurs at -2.76 , -1.73 , -1.55 , and 0 eV. Moreover, interactions between only Au d, O p, and S p orbitals take place at -2.25 and 0.82 eV. Within the C_6H_6 system, the hybridization between the Au s, Au d, C p, and S p orbitals in the C_6H_6 system appears at -2.88 , 0 , 0.77 , and 0.85 eV, while the hybridization of only Au d, C p, and S p orbitals occurs at -2.56 , -2.32 , -2.2 , and -1.72 eV. For the C_5H_8 system, the Au d and C p orbitals hybridize at -2.63 and -2.18 eV. Furthermore, aligning with our band structure results, the PDOS charts for all three systems exhibit electron states around the Fermi level, underscoring the metallic nature of each system. Simultaneously, the hybridization of different electron orbitals indicates a strong interaction between the three VOC molecules and the Au- SnS_2 monolayer, which agrees with our obtained strong adsorption energy.

The charge transfer isosurfaces between the VOC molecules and the Au- SnS_2 substrate are plotted in Figure 6, using eq 2. Electrons accumulate in the light blue area, while electron deficiency is evident in the pink region. From all three systems,

Table 4. Adsorption Energy (E_a), Binding Distance (h) between the VOC Gas and the Monolayer, Band Gap (E_g), and Recovery Time (τ) for All VOC Molecules Adsorbed on 4×4 Au- SnS_2 Monolayer

system	E_a (eV)	h (Å)	E_g (eV)	τ (s)
Au- SnS_2	N/A	N/A	0.035	N/A
C_3H_6O on Au- SnS_2	-0.77	2.13	0	8.63
C_6H_6 on Au- SnS_2	-0.717	2.32	0	1.11
C_5H_8 on Au- SnS_2	-1.313	2.16	0	1.14×10^{10}

we can identify a significant overlap between the light blue and pink regions, indicating a significant exchange of electrons. It is identified that electrons are mainly transferred from the Au dopant to the O or C atoms in the VOC molecule, indicating Au's electron donor behavior. Such results imply a strong interaction between the three VOC molecules and the Au- SnS_2 monolayer, which is consistent with the large adsorption energy shown in Table 4.

3.3. VOCs on Pd- SnS_2 . According to prior research,⁷² the most stable configuration involves the interstitial doping of a Pd atom at the hollow site, exhibiting an adsorption energy of -6.02 eV. This arrangement has been shown to significantly bolster the sensing capabilities of the original SnS_2 monolayer. Figure 2c displays the top and side views of the most stable configuration of the Pd- SnS_2 monolayer. The three Pd-S bonds are 2.38, 2.38, and 2.39 Å, while the lattice constant is slightly stretched to 3.72 Å, as shown in Table 2.

The optimized structures of the three VOC gases adsorbed on the Pd- SnS_2 substrate are demonstrated in Figure 7. As shown in Table 5, the computed adsorption energies for C_3H_6O , C_6H_6 , and C_5H_8 on Pd- SnS_2 are -0.53 , -0.561 , and

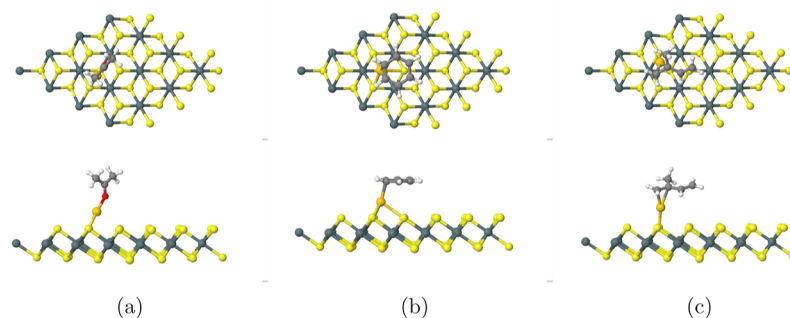


Figure 4. Top and side views of the optimized configurations of (a) C_3H_6O , (b) C_6H_6 , and (c) C_5H_8 adsorption on the Au- SnS_2 monolayer correspondingly. C, H, O, Sn, S, and Au are represented by light gray, white, red, dark gray, yellow, and light orange colors, respectively.

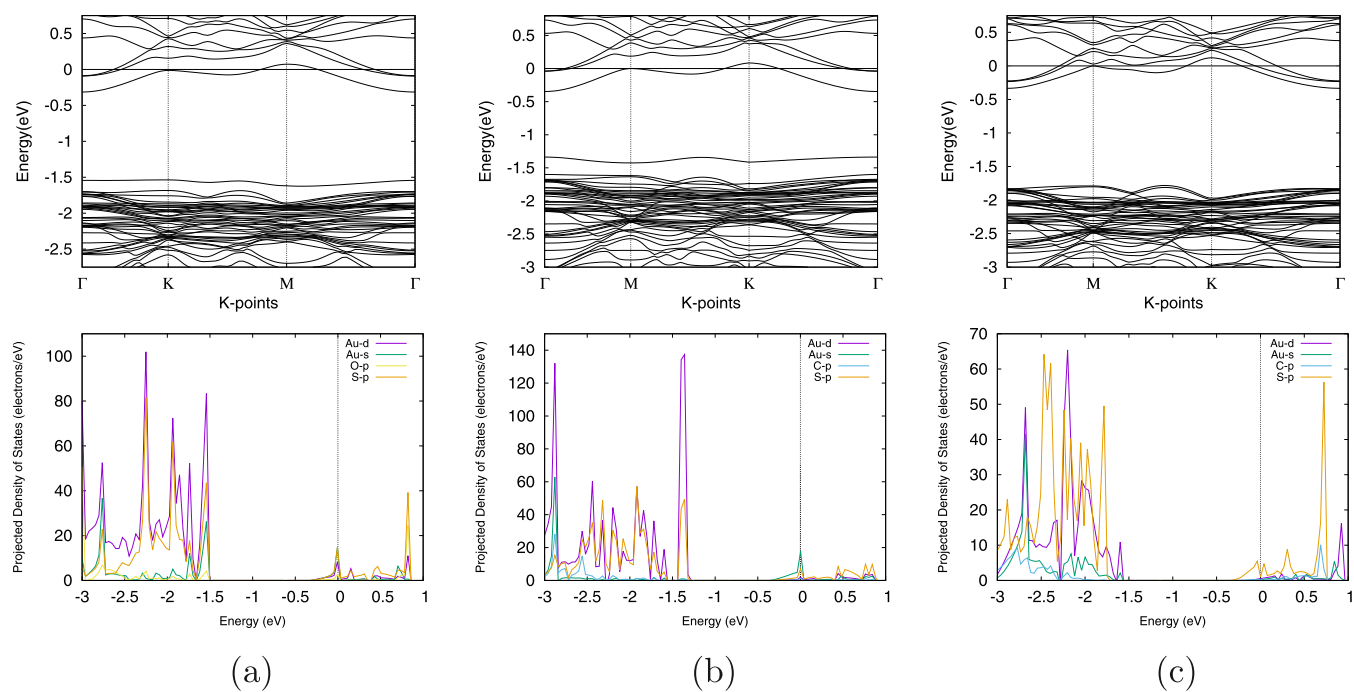


Figure 5. Band structure and PDOS of (a) C_3H_6O , (b) C_6H_6 , and (c) C_5H_8 on the Au–SnS₂ monolayer. Top row shows the band structures while the bottom row shows the PDOS of all systems. The Fermi level is set to 0. In the PDOS diagrams, Au d, Au s, C p, O p, and S p are represented by purple, green, light blue, yellow, and orange colors, respectively.

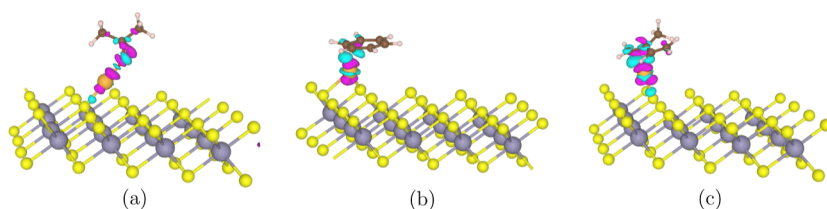


Figure 6. Charge transfer of (a) C_3H_6O , (b) C_6H_6 , and (c) C_5H_8 on an Au–SnS₂ monolayer. The light blue areas indicate electron accumulation, while the pink regions show electron depletion. The isosurface value is set to 0.005 electrons per Å³. Meanwhile, the yellow, gray, light orange, brown, white, and red colors represent S, Sn, Au, C, H, and O atoms, respectively.

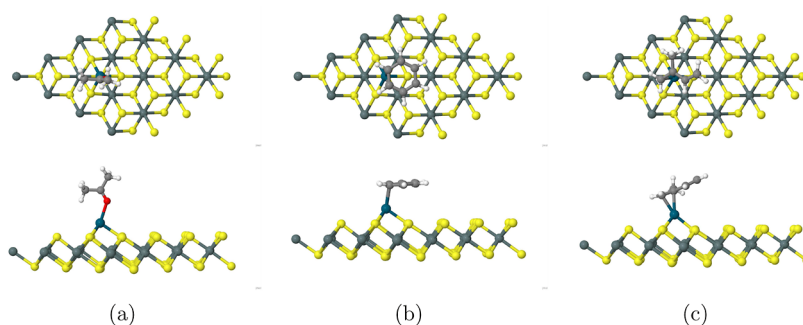


Figure 7. Top and side views of the most stable configurations of (a) C_3H_6O , (b) C_6H_6 , and (c) C_5H_8 adsorption on the Pd–SnS₂ monolayer correspondingly. C, H, O, Sn, S, and Pd are represented by light gray, white, red, dark gray, yellow, and blue-green colors respectively.

Table 5. Adsorption Energy (E_a), Binding Distance (h) between the VOC Gas and the Monolayer, Band Gap (E_g), and Recovery Time (τ) for All VOCs Adsorbed on 4 × 4 Pd–SnS₂ Monolayer

system	E_a (eV)	h (Å)	E_g (eV)	τ (s)
C_3H_6O on Pd–SnS ₂	−0.53	2.27	0.422	8.016×10^{-4}
C_6H_6 on Pd–SnS ₂	−0.561	2.4	0.378	2.66×10^{-3}
C_5H_8 on Pd–SnS ₂	−0.786	2.23	0.202	16.02

−0.786 eV, correspondingly. Meanwhile, the binding distances between the C_3H_6O , C_6H_6 , and C_5H_8 molecules, and the monolayer were measured to be 2.27, 2.4, and 2.23 Å. The results for adsorption energy and binding distances indicate that VOC adsorption on Pd–SnS₂ is stronger than that of pristine SnS₂ while slightly weaker than that of Au–SnS₂. Using eq 3, the obtained recovery times of C_3H_6O , C_6H_6 , and C_5H_8 from Pd–SnS₂ monolayer are 8×10^{-4} , 2.66×10^{-3} , and 16.02 s, respectively, which are significantly shorter than VOC

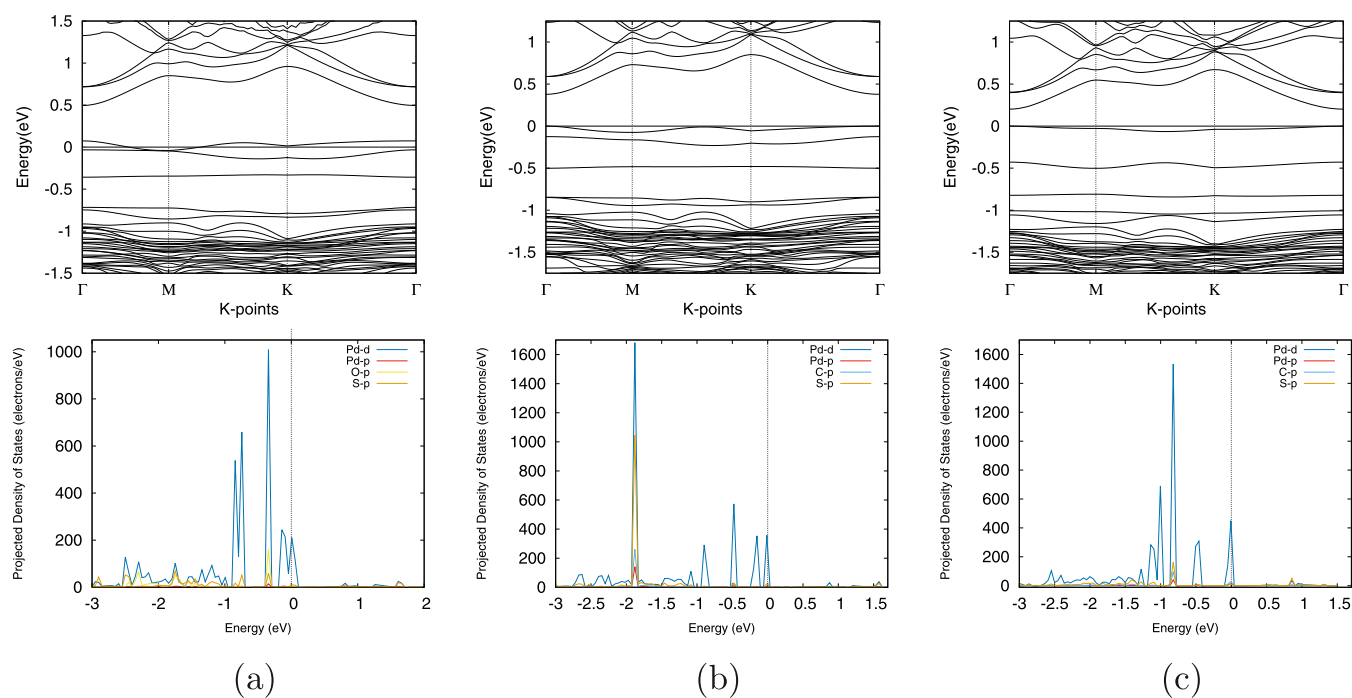


Figure 8. Band structure and PDOS of (a) C_3H_6O , (b) C_6H_6 , and (c) C_5H_8 on the Pd–SnS₂ monolayer. Top row shows the band structures while the bottom row shows the PDOS of all systems. The Fermi level is set to 0. In the PDOS diagrams, Pd d, Pd p, C p, O p, and S p are represented by dark blue, red, light blue, yellow, and orange colors respectively.

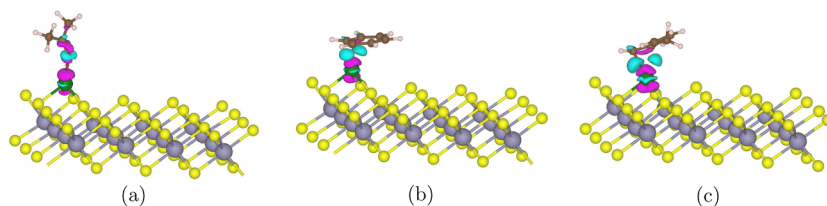


Figure 9. Charge transfer of (a) C_3H_6O , (b) C_6H_6 , and (c) C_5H_8 on a Pd–SnS₂ monolayer. The light blue areas indicate electron accumulation, while the pink regions show electron depletion. The isosurface value is set to 0.004 electrons per Å³. Meanwhile, the yellow, gray, green, brown, white, and red colors represent S, Sn, Pd, C, H, and O atoms respectively.

desorption from Au–SnS₂. Therefore, the Pd–SnS₂ monolayer offers enhanced desorption of the three VOCs compared to the Au–SnS₂ monolayer, inferring Pd–SnS₂ as a viable candidate for a reversible sensor.

After structural optimization, the band structures of Pd–SnS₂ before and after the adsorption of three VOC molecules were calculated, as identified in Figure 2c and the upper row of Figure 8. As illustrated in Table 2, after Pd is doped, the monolayer's band gap experiences a significant reduction from 1.59 to 0.57 eV. From Table 5, the band gaps of C_3H_6O , C_6H_6 , and C_5H_8 on Pd–SnS₂ are 0.422, 0.378, and 0.202 eV, respectively. In other words, the band gap of Pd–SnS₂ decreases by 0.148, 0.192, and 0.368 eV after interaction with C_3H_6O , C_6H_6 , and C_5H_8 molecules correspondingly. This signifies that the adsorption of volatile organic compounds (VOCs) induces substantial alterations in the band structures near the Fermi level. Meanwhile, in all three systems, the band structures exhibit a direct band gap with both the valence band maximum and conduction band minimum situated at the Γ point. From eq 4, we can deduce that the band gap plays a pivotal role in determining a monolayer's electrical conductivity. Therefore, the C_5H_8 system exhibits the highest conductivity due to its most significant reduction in the band gap, while the C_3H_6O system displays the lowest conductivity

among the three systems. The greatest shift in conductivity, according to eq 5, results in the highest sensing response for Pd–SnS₂ in the presence of C_5H_8 , with a remarkable 99.9%. This is followed by the C_6H_6 system at 97.56%, and last, the C_3H_6O system at 94.29%. These positive values of sensing response align with an increase in conductivity, a substantial decrease in the band gap, and strong adsorption energy. In contrast to Au–SnS₂, which elicits a minor alteration in the band gap upon gas adsorption, Pd–SnS₂ showcases a higher sensing response to C_3H_6O , C_6H_6 , and C_5H_8 due to its greater decrease in the band gap.

In addition, the PDOS after adsorption of the three VOC gas molecules on Pd–SnS₂ was also investigated, as shown in the bottom row of Figure 8. For C_3H_6O adsorption, electron hybridization between Pd d, Pd p, O p, and S p orbital occurs at -0.34 and 0 eV, while interactions between only Pd d, O p, and S p orbital happen at -2.31 , -1.76 , and 0.74 eV. In the C_6H_6 system, electron hybridization among Pd d, Pd p, O p, and S p orbitals is present at energy levels of -0.34 and 0 eV. While Pd d, O p, and S p orbitals hybridize at -2.31 , -1.76 , and 0.74 eV. Within the C_5H_8 configuration, electron hybridization among Pd d, Pd p, C p, and S p orbitals arises at energy levels of -0.85 , 0 , and 0.86 eV. Simultaneously, interactions of only Pd d, O p, and S p orbitals are located at

–2, 6, and –1.64 eV. The overlapping peaks at the Fermi level implicate a substantial change in the electronic properties of the Pd–SnS₂ monolayer and a significant increase in conductivity after VOC adsorption. Therefore, these results suggest a significant exchange of electrons between the C or the O atom from the three VOC molecules and the Pd dopant, which verifies the high adsorption energies and sensing responses that are present in all systems.

Using eq 2, the charge transfer isosurfaces between the three VOCs and the Pd–SnS₂ monolayer are shown in Figure 9. Similar to the adsorption on Au–SnS₂, electrons deplete around the Pd dopant and accumulate close to the O or C atoms in the VOC molecules for all three systems. Here, we can witness a significant exchange of electrons between the VOC molecules and the Pd-doped SnS₂ monolayer, which aligns with our results of the significant adsorption energy.

4. CONCLUSIONS

In summary, we employed first-principles calculations based on DFT to examine the adsorption and electronic characteristics of C₃H₆O, C₆H₆, and C₃H₈ on pristine Au- and Pd-doped SnS₂ monolayers. The reliability of a sensor depends on multiple factors, including moderate adsorption energy, rapid recovery time, and high sensing response toward the gas molecule. Our obtained results of adsorption energy and binding distance suggest that the strength adsorption upon the three VOC molecules is in the order of Au-doped, Pd-doped, and pure SnS₂ monolayer, from the strongest to the weakest. The recovery times for C₃H₆O, C₆H₆, and C₃H₈ adsorption on Pd–SnS₂ monolayer are smaller than that of Au–SnS₂, inferring Pd–SnS₂'s better potential for reversible sensors. Moreover, our analysis of electronic properties confirms that the sensing responses of Pd–SnS₂ upon the three VOC molecules are higher than that of the Au–SnS₂ monolayer. Thus, we conclude that the Pd–SnS₂ monolayer is a more promising potential for lung cancer VOC detection over pristine and Au–SnS₂ monolayer. Additional investigations should prioritize assessing Pd–SnS₂'s overall adsorption capacity and operational efficiency to gain insights into their energy consumption and purity levels following the capture of C₃H₆O, C₆H₆, and C₃H₈ molecules.

AUTHOR INFORMATION

Corresponding Author

Xuan Luo – National Graphene Research and Development Center, Springfield, Virginia 22151, United States;
orcid.org/0000-0002-0592-0610; Email: xluo@ngrd.org

Author

Hongyi Liu – National Graphene Research and Development Center, Springfield, Virginia 22151, United States;
orcid.org/0009-0008-1019-6496

Complete contact information is available at:
<https://pubs.acs.org/10.1021/acsomega.3c06346>

Notes

The authors declare no competing financial interest.

ACKNOWLEDGMENTS

We would like to thank Dr. Geifei Qian for providing technological support for this study. There was no financial assistance received for this study.

REFERENCES

- (1) Chaitanya Thandra, K.; Barsouk, A.; Saginala, K.; Sukumar Aluru, J.; Barsouk, A. Epidemiology of lung cancer. *Contemp. Oncol.* **2021**, *25*, 45–52.
- (2) Barta, J. A.; Powell, C. A.; Wisnivesky, J. P. Global Epidemiology of Lung Cancer. *Ann. Glob. Health* **2019**, *85*, 8.
- (3) Sung, H.; Ferlay, J.; Siegel, R. L.; Laversanne, M.; Soerjomataram, I.; Jemal, A.; Bray, F. Global cancer statistics 2020: GLOBOCAN estimates of incidence and mortality worldwide for 36 cancers in 185 countries. *Ca-Cancer J. Clin.* **2021**, *71*, 209–249.
- (4) Wan, Q.; Chen, X.; Xiao, S. Ru-Doped PtTe₂ Monolayer as a Promising Exhaled Breath Sensor for Early Diagnosis of Lung Cancer: A First-Principles Study. *Chemosensors* **2022**, *10*, 428.
- (5) Swensen, S. J.; Jett, J. R.; Hartman, T. E.; Midthun, D. E.; Mandrekar, S. J.; Hillman, S. L.; Sykes, A.; Aughenbaugh, G. L.; Bungum, A. O.; Allen, K. L. CT Screening for Lung Cancer: Five-year Prospective Experience. *Radiology* **2005**, *235*, 259–265.
- (6) Zia, K.; Siddiqui, T.; Ali, S.; Farooq, I.; Zafar, M. S.; Khurshid, Z. Nuclear magnetic resonance spectroscopy for medical and dental applications: a comprehensive review. *Eur. J. Dent.* **2019**, *13*, 124–128.
- (7) Altintas, Z.; Tothill, I. Biomarkers and biosensors for the early diagnosis of lung cancer. *Sens. Actuators, B* **2013**, *188*, 988–998.
- (8) Wan, Q.; Chen, X.; Gui, Y. First-principles insight into a Ru-doped SnS₂ monolayer as a promising biosensor for exhale gas analysis. *ACS Omega* **2020**, *5*, 8919–8926.
- (9) Barash, O.; Tisch, U.; Haick, H. Volatile organic compounds and the potential for a lung cancer breath test. *Lung Cancer Manag.* **2013**, *2*, 471–482.
- (10) Zhao, G.; Li, M. Ni-doped MoS₂ biosensor: a promising candidate for early diagnosis of lung cancer by exhaled breathe analysis. *Appl. Phys. A: Mater. Sci. Process.* **2018**, *124*, 751.
- (11) Das, S.; Pal, M. Non-invasive monitoring of human health by exhaled breath analysis: A comprehensive review. *J. Electrochem. Soc.* **2020**, *167*, 037562.
- (12) Aghaei, S.; Aasi, A.; Farhangdoust, S.; Panchapakesan, B. Graphene-like BC₆N nanosheets are potential candidates for detection of volatile organic compounds (VOCs) in human breath: A DFT study. *Appl. Surf. Sci.* **2021**, *536*, 147756.
- (13) Hakim, M.; Broza, Y. Y.; Barash, O.; Peled, N.; Phillips, M.; Amann, A.; Haick, H. Volatile organic compounds of lung cancer and possible biochemical pathways. *Chem. Rev.* **2012**, *112*, 5949–5966.
- (14) Saalberg, Y.; Wolff, M. VOC breath biomarkers in lung cancer. *Clin. Chim. Acta* **2016**, *459*, 5–9.
- (15) Liu, T.; Cui, Z.; Li, X.; Cui, H.; Liu, Y. Al-doped MoSe₂ monolayer as a promising biosensor for exhaled breath analysis: a DFT study. *ACS Omega* **2021**, *6*, 988–995.
- (16) Chatterjee, S.; Castro, M.; Feller, J.-F. An e-nose made of carbon nanotube based quantum resistive sensors for the detection of eighteen polar/nonpolar VOC biomarkers of lung cancer. *J. Mater. Chem. B* **2013**, *1*, 4563–4575.
- (17) Zhu, A.; Luo, X. Detection of covid-19 through a heptanal biomarker using transition metal doped graphene. *J. Phys. Chem. B* **2022**, *126*, 151–160.
- (18) Dewulf, J.; Van Langenhove, H.; Wittmann, G. Analysis of volatile organic compounds using gas chromatography. *TrAC, Trends Anal. Chem.* **2002**, *21*, 637–646.
- (19) Wang, K.; Luo, X. Transition-Metal-Doped SiP₂ Monolayer for Effective CO₂ Capture: A Density Functional Theory Study. *ACS Omega* **2022**, *7*, 36848–36855.
- (20) Wan, Q.; Xu, Y.; Zhang, X. Adsorption properties of typical lung cancer breath gases on Ni-SWCNTs through density functional theory. *J. Sens.* **2017**, *2017*, 1–8.
- (21) Tung, T. T.; Tran, M. T.; Feller, J.-F.; Castro, M.; Van Ngo, T.; Hassan, K.; Nine, M. J.; Losic, D. Graphene and metal organic frameworks (MOFs) hybridization for tunable chemoresistive sensors for detection of volatile organic compounds (VOCs) biomarkers. *Carbon* **2020**, *159*, 333–344.

- (22) Wang, W.; Zhang, Q.; Lv, R.; Wu, D.; Zhang, S. Enhancing formaldehyde selectivity of SnO₂ gas sensors with the ZSM-5 modified layers. *Sensors* **2021**, *21*, 3947.
- (23) Wu, X.; Wang, H.; Wang, J.; Chen, J.; Shi, L.; Han, B.; Tian, X. Hydrothermal synthesis of flower-like Cr₂O₃-doped In₂O₃ nanorods clusters for ultra-low isoprene detection. *Colloids Surf., A* **2021**, *620*, 126606.
- (24) Shavanova, K.; Bakakina, Y.; Burkova, I.; Shteplyuk, I.; Viter, R.; Ubelis, A.; Beni, V.; Starodub, N.; Yakimova, R.; Khranovskyy, V. Application of 2D non-graphene materials and 2D oxide nanostructures for biosensing technology. *Sensors* **2016**, *16*, 223.
- (25) Majidi, R.; Nadafan, M. Detection of exhaled gas by γ -graphyne and twin-graphene for early diagnosis of lung cancer: A density functional theory study. *Phys. Lett. A* **2020**, *384*, 126036.
- (26) Majidi, R.; Nadafan, M. Application of nitrogenated holey graphene for detection of volatile organic biomarkers in exhaled breath of humans with chronic kidney disease: a density functional theory study. *J. Comput. Electron.* **2021**, *20*, 1930–1937.
- (27) Li, Y.; Yu, C.-M. DFT study of the adsorption of C₆H₆ and C₆H₅OH molecules on stanene nanosheets: Applications to sensor devices. *Phys. E* **2021**, *127*, 114533.
- (28) Wang, X.; Liu, H.; Tu, S.-T. Study of formaldehyde adsorption on silicene with point defects by DFT method. *RSC Adv.* **2015**, *5*, 65255–65263.
- (29) Lam, P. T.; Luong, T. T.; On, V. V.; Dinh Van, A. DFT Study on Adsorption of Acetone and Toluene on Silicene. *VNU J. Sci.: Math.-Phys.* **2020**, *36*, 95–102.
- (30) Wan, Q.; Xu, Y.; Zhang, X. Adsorption Mechanism of Typical Gases Exhaled by Lung Cancer Patients on the Anatase TiO₂ (101) Surface. *J. Sens.* **2018**, *2018*, 1–7.
- (31) Masikini, M.; Chowdhury, M.; Nemraoui, O. Metal oxides: Application in exhaled breath acetone chemiresistive sensors. *J. Electrochem. Soc.* **2020**, *167*, 037537.
- (32) Tomić, M.; Šetka, M.; Vojkúvka, L.; Vallejos, S. VOCs sensing by metal oxides, conductive polymers, and carbon-based materials. *Nanomaterials* **2021**, *11*, 552.
- (33) Choi, W.; Choudhary, N.; Han, G. H.; Park, J.; Akinwande, D.; Lee, Y. H. Recent development of two-dimensional transition metal dichalcogenides and their applications. *Mater. Today* **2017**, *20*, 116–130.
- (34) Cui, H.; Zhang, X.; Zhang, G.; Tang, J. Pd-doped MoS₂ monolayer: a promising candidate for DGA in transformer oil based on DFT method. *Appl. Surf. Sci.* **2019**, *470*, 1035–1042.
- (35) Huang, L.; Lu, D.; Zeng, W.; Zhou, Q. Pt-Doped HfS₂ Monolayer as a Novel Sensor and Scavenger for Dissolved Gases (H₂, CO₂, CH₄, and C₂H₂) in Transformer Oil: A Density Functional Theory Study. *Langmuir* **2023**, *39*, 12920–12930.
- (36) Jiang, T.; He, Q.; Bi, M.; Chen, X.; Sun, H.; Tao, L. First-principles calculations of adsorption sensitivity of Au-doped MoS₂ gas sensor to main characteristic gases in oil. *J. Mater. Sci.* **2021**, *56*, 13673–13683.
- (37) Qian, G.; Peng, Q.; Zou, D.; Wang, S.; Yan, B.; Zhou, Q. First-principles insight into Au-doped MoS₂ for sensing C₂H₆ and C₂H₄. *Front. Mater.* **2020**, *7*, 22.
- (38) Zhang, X.; Teng, S. Y.; Loy, A. C. M.; How, B. S.; Leong, W. D.; Tao, X. Transition metal dichalcogenides for the application of pollution reduction: A review. *Nanomaterials* **2020**, *10*, 1012.
- (39) Cui, H.; Jia, P.; Peng, X.; Li, P. Adsorption and sensing of CO and C₂H₂ by S-defected SnS₂ monolayer for DGA in transformer oil: A DFT study. *Mater. Chem. Phys.* **2020**, *249*, 123006.
- (40) Guo, S.; Hu, X.; Huang, Y.; Zhou, W.; Qu, H.; Xu, L.; Song, X.; Zhang, S.; Zeng, H. A highly sensitive and selective SnS₂ monolayer sensor in detecting SF₆ decomposition gas. *Appl. Surf. Sci.* **2021**, *541*, 148494.
- (41) Song, H.; Li, S.; Gao, L.; Xu, Y.; Ueno, K.; Tang, J.; Cheng, Y.; Tsukagoshi, K. High-performance top-gated monolayer SnS₂ field-effect transistors and their integrated logic circuits. *Nanoscale* **2013**, *5*, 9666–9670.
- (42) Peng, R.; Zeng, W.; Zhou, Q. Adsorption and gas sensing of dissolved gases in transformer oil onto Ru₃-modified SnS₂: A DFT study. *Appl. Surf. Sci.* **2023**, *615*, 156445.
- (43) Ou, J. Z.; Ge, W.; Carey, B.; Daeneke, T.; Rotbart, A.; Shan, W.; Wang, Y.; Fu, Z.; Chrimes, A. F.; Wlodarski, W.; et al. Physisorption-based charge transfer in two-dimensional SnS₂ for selective and reversible NO₂ gas sensing. *ACS Nano* **2015**, *9*, 10313–10323.
- (44) Zhao, R.; Wang, T.; Zhao, M.; Xia, C.; Zhao, X.; An, Y.; Dai, X. A theoretical simulation of small-molecules sensing on an S-vacancy SnS₂ monolayer. *Phys. Chem. Chem. Phys.* **2017**, *19*, 10470–10480.
- (45) Wang, X.; Wang, J. Effects of Pt and Au adsorption on the gas sensing performance of SnS₂ monolayers: A DFT study. *Mater. Sci. Semicond. Process.* **2021**, *121*, 105416.
- (46) Ma, S.; Jin, Y.; Si, Y. Adsorption behavior of Pd-doped SnS₂ monolayer upon H₂ and C₂H₂ for dissolved gas analysis in transformer oil. *Adsorption* **2019**, *25*, 1587–1594.
- (47) Gui, Y.; Hu, X.; Zhu, S.; Chen, X. A DFT study of transition metal (Ag, Au, Co) modified SnS₂ monolayer for the detection and adsorption of the representative gases (NH₃, Cl₂, and C₂H₂) in greenhouses. *Mater. Today Commun.* **2022**, *33*, 104618.
- (48) Chen, J.; Zhou, Q.; Jia, L.; Cui, X.; Zeng, W. The gas-sensing mechanism of Pt₃ cluster doped SnS₂ monolayer for SF₆ decomposition: A DFT study. *Appl. Surf. Sci.* **2022**, *597*, 153693.
- (49) Nesbet, R. Reference-state density functional theory. *J. Phys. Chem.* **1996**, *100*, 6104–6106.
- (50) Gonze, X.; Amadon, B.; Anglade, P. M.; Beuken, J. M.; Bottin, F.; Boulanger, P.; Bruneval, F.; Caliste, D.; Caracas, R.; Côté, M.; et al. ABINIT: First-principles approach of materials and nanosystem properties. *Comput. Phys. Commun.* **2009**, *180*, 2582–2615.
- (51) Perdew, J. P.; Burke, K.; Ernzerhof, M. Generalized Gradient Approximation Made Simple. *Phys. Rev. Lett.* **1996**, *77*, 3865–3868.
- (52) Blochl, P. E. Projector augmented-wave method. *Phys. Rev. B: Condens. Matter Mater. Phys.* **1994**, *50*, 17953–17979.
- (53) Holzwarth, N.; Tackett, A.; Matthews, G. A Projector Augmented Wave (PAW) code for electronic structure calculations, Part I: atom-paw for generating atom-centered functions. *Comput. Phys. Commun.* **2001**, *135*, 329–347.
- (54) Monkhorst, H. J.; Pack, J. D. Special points for Brillouin-zone integrations. *Phys. Rev. B: Solid State* **1976**, *13*, 5188–5192.
- (55) Head, J. D.; Zerner, M. C. A Broyden–Fletcher–Goldfarb–Shanno optimization procedure for molecular geometries. *Chem. Phys. Lett.* **1985**, *122*, 264–270.
- (56) Zhang, J.; Feng, W.; Zhang, Y.; Zeng, W.; Zhou, Q. Gas-sensing properties and first-principles comparative study of metal (Pd, Pt)-decorated MoSe₂ hierarchical nanoflowers for efficient SO₂ detection at room temperature. *J. Alloys Compd.* **2023**, *968*, 172006.
- (57) Lu, D.; Huang, L.; Zhang, J.; Zhang, Y.; Feng, W.; Zeng, W.; Zhou, Q. Rh- and Ru-Modified InSe Monolayers for Detection of NH₃, NO₂, and SO₂ in Agricultural Greenhouse: A DFT Study. *ACS Appl. Nano Mater.* **2023**, *6*, 14447–14458.
- (58) Shi, Z.; Zhang, Y.; Zeng, W.; Zhou, Q. A DFT study on adsorption of SF₆ decomposition gases (H₂S, SO₂, SO₂F₂ and SOF₂) on Sc-MoTe₂ monolayer. *Sens. Actuators, A* **2023**, *360*, 114548.
- (59) Lu, D.; Zhang, Y.; Feng, W.; Zeng, W.; Zhou, Q. Experimental and theoretical comparative analysis of modified graphene (GO, Pd-G, Pd-GO) sensing performance toward SO₂ in agricultural greenhouse. *Ceram. Int.* **2023**, *49*, 26516–26529.
- (60) Li, Z.; Liao, Y.; Liu, Y.; Zeng, W.; Zhou, Q. Room temperature detection of nitrogen dioxide gas sensor based on Pt-modified MoSe₂ nanoflowers: Experimental and theoretical analysis. *Appl. Surf. Sci.* **2023**, *610*, 155527.
- (61) Wang, M.; Zhou, Q.; Zeng, W. Theoretical study on adsorption of SF₆ decomposition gas in GIS gas cell based on intrinsic and Ni-doped MoTe₂ monolayer. *Appl. Surf. Sci.* **2022**, *591*, 153167.
- (62) Wang, J.; Zhou, Q.; Lu, Z.; Wei, Z.; Zeng, W. Gas sensing performances and mechanism at atomic level of Au-MoS₂ microspheres. *Appl. Surf. Sci.* **2019**, *490*, 124–136.

(63) Chen, J.; Chen, J.; Zeng, W.; Zhou, Q. Adsorption of HCN on WSe₂ monolayer doped with transition metal (Fe, Ag, Au, As and Mo). *Sens. Actuators, A* **2022**, *341*, 113612.

(64) Wang, J.; Zhou, Q.; Wei, Z.; Xu, L.; Zeng, W. Experimental and theoretical studies of Zn-doped MoO₃ hierarchical microflower with excellent sensing performances to carbon monoxide. *Ceram. Int.* **2020**, *46*, 29222–29232.

(65) Cai, Y.; Luo, X. First-principles investigation of carbon dioxide adsorption on MN₄ doped graphene. *AIP Adv.* **2020**, *10*, 125013.

(66) Liu, C.; Luo, X. Potential molecular and graphene oxide chelators to dissolve amyloid- β plaques in Alzheimer's disease: a density functional theory study. *J. Mater. Chem. B* **2021**, *9*, 2736–2746.

(67) Bastiansen, O.; Viervoll, H.; Gjertsen, P. A comparison between the structures of acetone and methyl sulfoxide. *Acta Chem. Scand.* **1948**, *2*, 702–706.

(68) Dzade, N. Y.; Roldan, A.; De Leeuw, N. H. A density functional theory study of the adsorption of benzene on hematite (α -Fe₂O₃) surfaces. *Minerals* **2014**, *4*, 89–115.

(69) Stevens, P. S.; Seymour, E.; Li, Z. Theoretical and experimental studies of the reaction of OH with isoprene. *J. Phys. Chem. A* **2000**, *104*, 5989–5997.

(70) Zhen, Z.-Q.; Wang, H.-Y. Density functional study of the electronic, elastic, and lattice dynamic properties of SnS₂. *Acta Phys. Polym., A* **2020**, *137*, 1095–1100.

(71) Ali, A.; Zhang, J.-M.; Muhammad, I.; Shahid, I.; Ahmad, I.; Rehman, M. U.; Ahmad, I.; Kabir, F. First-principles investigation on electronic structure, magnetic states and optical properties of Mn-doped SnS₂ monolayer via strain engineering. *Phys. E* **2021**, *134*, 114842.

(72) Chi, S.; Luan, T.; Liang, Y.; Gao, Y.; Zhang, Y. A DFT study of the adsorption of noble metal adatoms (Pd, Pt, Ag, Au) on 2D tin disulfide monolayers: Potential towards nanoscale electronic devices. *Phys. E* **2020**, *120*, 114080.